Blind Selection of Representative Observations for Sensor Radar Networks

Stefania Bartoletti, *Student Member, IEEE*, Andrea Giorgetti, *Senior Member, IEEE*, Moe Z. Win, *Fellow, IEEE*, and Andrea Conti, *Senior Member, IEEE*

***Abstract*—Sensor radar networks enable important new applications based on accurate localization. They rely on the quality of range measurements, which serve as observations for inferring a target location. In harsh propagation environments (e.g., indoors), such observations can be nonrepresentative of the target due to noise, multipath, clutter, and non-line-of-sight conditions leading to target misdetection, false-alarm events, and inaccurate localization. These conditions can be mitigated by selecting and processing a subset of representative observations. We introduce blind techniques for the selection of representative observations gathered by sensor radars operating in harsh environments. A methodology for the design and analysis of sensor radar networks is developed, taking into account the aforementioned impairments and observation selection. Results are obtained for noncoherent ultra-wideband sensor radars in a typical indoor environment (with obstructions, multipath, and clutter) to enable a clear understanding of how observation selection improves the localization accuracy.**

***Index Terms*—Diversity techniques, network localization, performance evaluation, representative observations, sensor radars.**

I. Introduction

LOCATION INFERENCE is essential for important new applications (e.g., in safety, imaging, military, and logistic sectors). Localization algorithms estimate the position of objects based on prior knowledge and on observations (measurements) gathered by a network of sensors deployed in the environment. In range-based localization, sensors provide range measurements whose reliability depends on the intrinsic properties of the network, such as the sensor positions and wireless medium [1]. From this perspective, localization accuracy and resource utilization may benefit from selecting and processing a subset of reliable observations instead of the entire set. This calls for observation selection techniques enabling high-accuracy localization with low complexity.

Range is determined from signals directly conveyed between objects (in unknown positions) and anchors (in known positions) or from signals emitted by anchors and backscattered by objects depending on their radar cross section (RCS):[1] The former is referred to as localization of active objects (tags), whereas the latter is referred to as localization of passive objects (targets). Typically, classification of localization systems uses the term "active" to indicate that the system emits a signal designed for target detection and localization, e.g., active radar, and the term "passive" to indicate that the system exploits signals emitted by other sources of opportunity, e.g., passive radar [2]–[5]. Hereafter, sensor radar (also known as multistatic radar) is referred to as a network of active radars in a monostatic or a bistatic configuration [6]–[9].[2]

Accurate localization via sensor radars is challenging in wireless environments with multipath, clutter, and signal obstructions (for example, caused by furniture and walls in indoor scenarios). These conditions can cause observations (e.g., range measurements) that are nonrepresentative of the target object (i.e., nonrepresentative outliers [10]) with a heavy impact on the localization accuracy. These conditions can be mitigated by using signals with large bandwidth, exploiting prior knowledge, and selecting representative observations [11]–[17].

Previous works on selection techniques for sensor radars aim to improve localization accuracy or to reduce signal processing complexity by choosing a subset of active sensors. In [18], the subset of active antennas employed in the localization process is minimized by selecting only those that fulfill the required performance. In [19] and [20], an approach based on Kalman filter for global and local node selection is proposed to increase geolocation accuracy in a distributed network of sensors. The node selection relies on a combinatorial optimization framework and on the use of the Cramér–Rao bound, which requires prior knowledge of the target position and signal-to-noise ratio (SNR) for each transmitter–target–receiver link.

Sensor radars based on ultra-wideband (UWB) signals [21]–[23] can provide accurate localization in harsh propagation environments due to their ability to resolve multipath

Manuscript received May 16, 2014; revised October 15, 2014; accepted December 19, 2014. Date of publication January 27, 2015; date of current version April 14, 2015. This work was supported in part by the Copernicus Fellowship, by the Italian MIUR through Project GRETA under Grant 2010WHY5PR and by the Office of Naval Research under Grant N00014-11-1-0397. The review of this paper was coordinated by Prof. D. Dardari, Dr. P. Closas, and Prof. P. M. Djurić.

S. Bartoletti and A. Conti are with the Dipartimento di Ingegneria (ENDIF), University of Ferrara, 44122 Ferrara, Italy (e-mail: stefania.bartoletti@unife.it; a.conti@ieee.org).

A. Giorgetti is with the Department of Electrical, Electronic and Information Engineering (DEI), University of Bologna, 40126 Bologna, Italy (e-mail: a.giorgetti@ieee.org).

M. Z. Win is with the Laboratory for Information and Decision Systems (LIDS), Massachusetts Institute of Technology, Cambridge, MA 02139 USA (e-mail: moewin@mit.edu).

Color versions of one or more of the figures in this paper are available online at http://ieeexplore.ieee.org.

Digital Object Identifier 10.1109/TVT.2015.2397312

[1]The RCS indicates how detectable a target is by measuring the power density it reflects with respect to the incident one, in relation to target orientation, material, and size.

[2]A radar is monostatic or bistatic when the transmitter and the receiver are colocated or dislocated, respectively.

and penetrate obstacles. Specifically, UWB signals provide fine delay resolution, which enables precise time-of-arrival (TOA) measurements for ranging [24]–[31]. However, the accuracy and reliability of range-based localization typically degrade in wireless environments with multipath, clutter, line-of-sight (LOS) blockage, and excess propagation delays through materials [32]–[39]. Sensor radars exploiting the characteristics of UWB signals are presented in [40]–[47].

Ranging accuracy in sensor radars depends on the capability of exploiting prior knowledge, noise filtering, clutter mitigation, and TOA estimation. A variety of range error models have been adopted in the literature [48].

The fundamental questions for the design of target localization techniques via sensor radars are the following: (i) What are the intrinsic properties of the sensor radar network dominating its performance in a given operation environment? (ii) How does the quality of the measurements impact the localization accuracy? (iii) How to conceive the network setting, waveform processing, and localization algorithm to mitigate propagation impairments? The answers to these questions enable the design of sensor radars exploiting the intrinsic properties of the network for a new level of localization accuracy, even in harsh propagation environments.

Our approach consists in exploiting diversity and selection of measurements to enhance the performance of sensor radars in harsh propagation environments with non-LOS (NLOS) conditions.[3] The goal of this work is to provide insights into how the network intrinsic properties, the waveform processing, and the localization algorithm affect detection and localization capabilities of sensor radars, as well as to demonstrate that proper techniques for selecting a subset of observations can improve the localization accuracy, despite the lower complexity.

In this paper, we propose techniques that are blind to both channel knowledge and propagation environment for selecting representative observations. Such blind techniques rely on indicators obtained from noncoherent reception and sub-Nyquist sampling of waveforms. We develop a methodology for the design and analysis of sensor radar by jointly considering network intrinsic properties and signal processing techniques. The key contributions of this paper can be summarized as follows:

- introduction of blind techniques for the selection of representative observations in sensor radars;
- development of a methodology for the design and analysis of sensor radars by jointly considering (i) network setting, (ii) propagation environment, (iii) waveform processing, (iv) observation selection, and (v) localization algorithm;
- quantification of the localization accuracy improvement provided by observation selection techniques.

The performance evaluation accounts for all the channel impairments such as multipath, clutter, and LOS/NLOS propagation. To understand the key benefits of selecting representative observations, we consider all the relevant aspects of the sensor radar and the propagation environments, neglecting synchronization errors and other secondary aspects that are beyond the scope of this study. Instead of considering a specific range error model, we simulate the entire signal processing chain starting from the received waveforms. As a case study, we consider UWB sensor radars in a typical indoor environment (with LOS and NLOS conditions, clutter, and multipath).

[3]Diversity is a well-known concept used in wireless communications to improve the performance, particularly in fading channels (see, e.g., [49]–[53]).

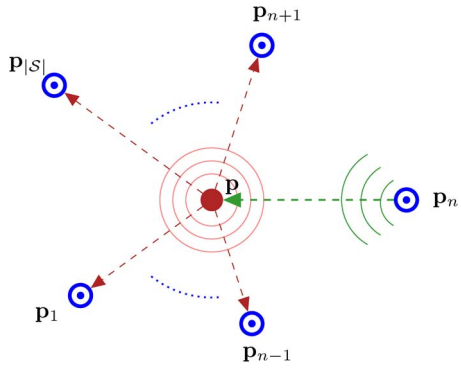

Fig. 1. Example of a sensor radar configuration with one transmitter at $\mathbf{p}_n$ and $|\mathcal{S}|-1$ receivers at $\mathbf{p}_1, \mathbf{p}_2, \ldots, \mathbf{p}_{n-1}, \mathbf{p}_{n+1}, \mathbf{p}_{n+2}, \ldots, \mathbf{p}_{|\mathcal{S}|}$; the target is at $\mathbf{p}$.

The remainder of this paper is organized as follows. Section II describes the sensor radar network. Section III introduces the collection and selection of representative observations. Section IV defines indicators and features for the observation selection. Section V presents the techniques for the processing of the received waveforms. Section VI provides results for a case study, and finally, Section VII gives our conclusions.

II. Sensor Radar Network

We now describe the network setting and the propagation environment for the analysis of sensor radars.

A. Network Setting

Refer to a network of sensors with index set $\mathcal{S}$ and cardinality $|\mathcal{S}|$, where the sensor indexed by $s \in \mathcal{S}$ is in position $\mathbf{p}_s$. The radar configuration is defined by an index subset $\mathcal{T} \subset \mathcal{S}$ of $|\mathcal{T}|$ transmitters and an index subset $\mathcal{R} \subset \mathcal{S}$ of $|\mathcal{R}|$ receivers. The ith transmitter ($i \in \mathcal{T}$) and the jth receiver ($j \in \mathcal{R}$) are at $\mathbf{p}_i$ and $\mathbf{p}_j$, respectively. Such a radar configuration defines an index set $\mathcal{P}$ of transmitter–receiver pairs with cardinality $|\mathcal{P}| = |\mathcal{T}| \times |\mathcal{R}|$. Specifically, each pair $(i,j) \in \mathcal{P}$ is composed of the ith transmitter emitting a signal and the jth receiver collecting the received signal after backscattering by the target object and wireless propagation. Fig. 1 shows an example of sensor radar with $\mathcal{P} = \{(n,1),(n,2),\ldots,(n,n-1),(n,n+1),\ldots,(n,|\mathcal{S}|)\}$. By processing the received signal for each pair, the TOA is estimated, and the transmitter-to-target-to-receiver distance (signal path length) is determined.

For a target object in position $\mathbf{p}$ and a radar $(i,j) \in \mathcal{P}$, the signal path length is given by

$$d_{ij}(\mathbf{p}) = d_i(\mathbf{p}) + d_j(\mathbf{p}) = \tau_{ij}(\mathbf{p})c \tag{1}$$

where $d_i(\mathbf{p})$ and $d_j(\mathbf{p})$ are the ith transmitter-to-target and target-to-jth receiver distances, respectively, c is the speed of light, and $\tau_{ij}(\mathbf{p})$ is the TOA at the jth receiver for a signal emitted by the ith transmitter and backscattered by the target.[4]

The transmitter–receiver pair forms a monostatic or a bistatic radar whether the transmitter and the receiver are colocated ($\mathbf{p}_i = \mathbf{p}_j$) or not ($\mathbf{p}_i \neq \mathbf{p}_j$).[5] In a bistatic radar, each single signal transmission causes the reception of at least two signal replicas in free-space propagation: the direct signal via the transmitter-to-receiver path and the reflected signal via the transmitter-to-target-to-receiver path [8]. Thus, a temporal separation between the two signal replicas is necessary to ensure their resolvability, which results in a minimum resolvable delay for the radar. In a monostatic radar, the same antenna is used for transmission and reception. Thus, a switching time between the transmission and reception phases is present, which results in a blind range for the radar. In the following, $\tau_{\min}$ denotes either the minimum resolvable delay and the blind range for the bistatic or monostatic case, respectively [7].

The TOA $\tau_{ij}(\mathbf{p})$ can be determined and the target detected by the radar $(i,j) \in \mathcal{P}$ if

$$d_{ij}(\mathbf{p}) \geq d_{ij}^{\star} \tag{2}$$

where $d_{ij}^{\star} = \|\mathbf{p}_i - \mathbf{p}_j\| + \tau_{\min} c$. Then, the target position can be determined by a localization algorithm that processes the observation vector $\hat{\boldsymbol{\tau}}_{\mathcal{P}}(\mathbf{p})$ with elements $\hat{\tau}_{ij}(\mathbf{p})$ representing the estimated TOA for all the radars $(i,j) \in \mathcal{P}$.

The detection and localization capabilities of a sensor radar network depend on its intrinsic properties, the receiver sensitivity, and the received SNRs. Specifically, the received SNR $\gamma_{ij}(\mathbf{p})$ for the radar $(i,j) \in \mathcal{P}$ and target at $\mathbf{p}$ is given by

$$\gamma_{ij}(\mathbf{p}) = \frac{P_{\mathrm{R},ij}(\mathbf{p})}{\mathsf{PRF} N_0} \tag{3}$$

where $P_{\mathrm{R},ij}(\mathbf{p})$ is the received power referred to a pulse repetition frequency (PRF) PRF, and N_0 is the one-sided power spectral density (PSD) of the noise. Target detection and TOA estimation benefit from gathering the energy of multiple backscattered signals. This gathering occurs by processing received signals collected from the transmission of N_{p} signals.

A minimum received SNR $\gamma^{\star}$ must be guaranteed to fulfill detection requirements. From (3), this requirement corresponds to a minimum received power $P_{\mathrm{R}}^{\star}$ as[6]

$$P_{\mathrm{R},ij}(\mathbf{p}) \geq P_{\mathrm{R}}^{\star}. \tag{4}$$

[4]It is known that the target position $\mathbf{p}$ is given by the intersection of isorange contours (the TOA estimates define circumference or ellipses in the monostatic and the bistatic case, respectively) [7]. In general, isorange contours have more points of intersection leading to ambiguities in target location in nonideal conditions.

[5]Note that bistatic pairs might require accurate phase and time synchronization between the transmitter and the receiver [7].

[6]The locus of points satisfying the minimum SNR requirement, in a bidimensional scenario with free-space propagation, corresponds to that inside a circumference (namely, maximum circumference) for monostatic radars and that inside a Cassini oval (namely, maximum Cassini oval) for bistatic radars [8]. In NLOS conditions, the area covered is irregular and depends on the obstructions of signal propagation.

B. Propagation Environment

The power received in a band $[f_{\mathrm{L}}, f_{\mathrm{U}}]$ from the ith transmitter-to-target-to-jth receiver path is given by

$$P_{\mathrm{R},ij}(\mathbf{p}) = \int_{f_{\mathrm{L}}}^{f_{\mathrm{U}}} R_{ij}(f,\mathbf{p}) df \tag{5}$$

where $R_{ij}(f,\mathbf{p})$ is the one-sided PSD of the received signal.

In free-space propagation (i.e., LOS conditions), the signal is attenuated due to the path loss. In obstructed propagation (i.e., NLOS conditions), in addition to the path loss, the signal is also attenuated and time-delayed by obstructions depending on the material characteristics such as the relative permittivity and attenuation coefficient. The obstruction loss $L_{ij}(f,\mathbf{p})$ accounts for such effects on the received signal PSD. In a general case, the received signal PSD is affected by path loss and obstruction loss as

$$R_{ij}(f,\mathbf{p}) = \frac{\overset{\circ}{R}_{ij}(f,\mathbf{p})}{L_{ij}(f,\mathbf{p})} \tag{6}$$

where $\overset{\circ}{R}_{ij}(f,\mathbf{p})$ is the received signal PSD in LOS conditions.

In the case of UWB signals, the path loss is modeled according to the IEEE 802.15.4a standard [54]. In particular, the one-sided PSD of the signal received for the radar $(i,j) \in \mathcal{P}$ and target at $\mathbf{p}$ in the absence of signal obstructions is given by

$$\overset{\circ}{R}_{ij}(f,\mathbf{p}) = \frac{T_i(f)\,\eta_i\,(f,\boldsymbol{\Theta}_i)\,\eta_j\,(f,\boldsymbol{\Theta}_j)\,\Sigma\,(f,\boldsymbol{\Theta}_i,\boldsymbol{\Theta}_j)}{(4\pi)^3 \left(\frac{f_0 d_0}{c}\right)^2 \ell_{ij}^{\beta}(\mathbf{p}) \left(\frac{f}{f_0}\right)^{2\kappa+2}} \tag{7}$$

where $T_i(f)$ is the transmitted signal PSD that feeds the transmitting antenna; d_0 is the reference distance and f_0 the center frequency; $\eta_i(f,\boldsymbol{\Theta}_i)$ and $\eta_j(f,\boldsymbol{\Theta}_j)$ are the transmitting and receiving antenna efficiencies, respectively; $\boldsymbol{\Theta}_i$ and $\boldsymbol{\Theta}_j$ are the solid angles between ith transmitter–target and target–jth receiver, respectively; $\Sigma(f,\boldsymbol{\Theta}_i,\boldsymbol{\Theta}_j)$ is the RCS of the target; and $\ell_{ij}(\mathbf{p}) = d_i(\mathbf{p}) d_j(\mathbf{p}) / {d_0}^2$. The path-loss exponents β and κ provide the path-loss dependence on distance and frequency, respectively. In a typical indoor environment, the presence of walls determines an NLOS condition with obstruction loss (in decibels) given by [55]

$$10 \log_{10} L_{ij}(f,\mathbf{p}) = \sum_{w=1}^{W_{ij}(\mathbf{p})} n_{ij}^{(w)}(\mathbf{p}) X^{(w)}(f) \tag{8}$$

where $W_{ij}(\mathbf{p})$ is the number of wall types met by the signal (incident and scattered), $n_{ij}^{(w)}(\mathbf{p})$ is the number of walls of type w, and $X^{(w)}(f)$ is the frequency-dependent loss induced by a wall of type w. Therefore, the total loss is the sum of path loss and obstruction loss located along the propagation paths. Note that $L_{ij}(f,\mathbf{p}) = 1$ in free-space propagation.

Together with the obstruction loss, the presence of obstacles and walls obstructing the signal path results in an excess delay for the TOA, which causes a positive bias on the TOA estimate. For example, a set of measurements was performed to characterize the excess delay on UWB signals due to the presence of concrete walls in a typical office building [38], showing that

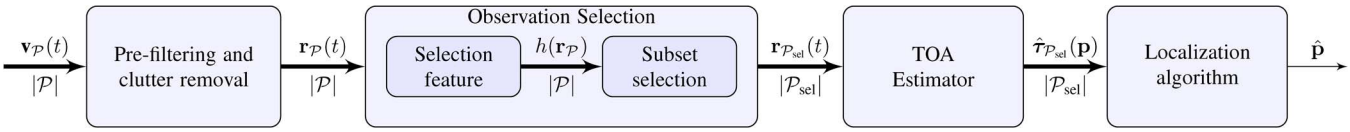

Fig. 2. Sensing and processing in sensor radar networks for localization with observation selection.

the TOA estimate bias is $\beta_{ij}(\mathbf{p}) \simeq \Delta/c$, where Δ is the total thickness of the wall.

The accuracy of target location inference relies on the quality of TOA estimates composing the observation vector $\hat{\boldsymbol{\tau}}_{\mathcal{P}}(\mathbf{p})$, which depends on the intrinsic properties of the sensor radar. The processing of signals received in LOS conditions might result in imperfect TOA estimation $\hat{\tau}_{ij}(\mathbf{p})$; therefore, in an imperfect signal path-length estimation, $\hat{d}_{ij}(\mathbf{p}) = \hat{\tau}_{ij}(\mathbf{p})c$, due to nonideal propagation (e.g., multipath, clutter, and noise). The processing of signals received in NLOS conditions might result in inaccurate TOA estimates due to excess delay and obstruction loss. Therefore, in NLOS conditions, the TOA estimates are more likely nonrepresentative observations of the target. Hence, given an observation vector obtained from diverse radars in the sensor radar network, the localization accuracy can be enhanced by processing a subset of representative observations of the target. Section V will present the processing techniques for the selection of representative observations in sensor radars.

III. Observation Collection and Selection

The range estimates serve as inputs of localization algorithms to determine the target position. Specifically, from the set $\mathcal{P}$ of transmitter–receiver pairs, a vector $\hat{\boldsymbol{\tau}}_{\mathcal{P}}(\mathbf{p})$ of $N_{\rm obs} = |\mathcal{P}| = |\mathcal{T}| \times |\mathcal{R}|$ observations collected in diverse spatiotemporal conditions is obtained for a target at $\mathbf{p}$. In inference theory, the presence of nonrepresentative and biased observations (also known as nonrepresentative outliers [10]) leads to inaccurate parameter estimation. Therefore, range estimates related to multipath, clutter, and signal obstructions degrade the accuracy of position estimation. We propose low-complexity techniques to select a subset $\hat{\boldsymbol{\tau}}_{\mathcal{P}_{\rm sel}}(\mathbf{p})$ of $L = |\mathcal{P}_{\rm sel}| \leq N_{\rm obs}$ elements of the observation vector that contains representative observations for the target position estimation. Such selection techniques are based on signal features that can be extracted in blind conditions (i.e., without prior information).

Fig. 2 shows the block scheme for target localization starting from the set of received signals $\mathbf{v}_{\mathcal{P}}(t) = \{v_{ij}(t) : (i,j) \in \mathcal{P}\}$. For each signal after prefiltering and clutter removal $r_{ij}(t)$, a feature $h(r_{ij})$ is extracted. Then, a subset of cardinality $L \leq N_{\rm obs}$ of vectors $\boldsymbol{r}_{\mathcal{P}_{\rm sel}}(t)$ is selected based on such a feature. The TOA estimator at each receiver determines $\hat{\tau}_{ij}$ for the signal $r_{ij}(t)$ if selected, i.e., $(i,j) \in \mathcal{P}_{\rm sel}$.

The target position is inferred based on the set of selected observations $\hat{\boldsymbol{\tau}}_{\mathcal{P}_{\rm sel}}(\mathbf{p}) \subseteq \hat{\boldsymbol{\tau}}_{\mathcal{P}}(\mathbf{p})$. Such a set of observations is processed by a Bayesian or a non-Bayesian localization algorithm. The choice of the localization algorithm is driven by the tradeoff between performance (such as localization error and outage) and complexity (such as computational complexity and message passing), as well as by prior knowledge of the environment. In this paper, no information on the bias introduced by obstructions, residual clutter after nonideal removal, nor TOA statistical distribution is available for position estimation. In such a blind case, a least squares (LS) estimator can be adopted, which is expressed as[7]

$$\hat{\mathbf{p}} = \arg\min_{\tilde{\mathbf{p}}} \sum_{(i,j)\in\mathcal{P}_{\rm sel}} \left|\hat{\tau}_{ij}(\mathbf{p}) - \tau_{ij}(\tilde{\mathbf{p}})\right|^2. \tag{9}$$

The choice of the processing techniques for the received signals impacts the quality of observations and the accuracy of location inference. The signal processing techniques considered in this paper, which consist of received waveform prefiltering and clutter removal, as well as TOA estimation, will be described in Section V.

We now determine the localization complexity in the presence of observation selection, i.e., $\mathcal{C}(L, N_{\rm obs})$, where L is the number of selected observations, and $N_{\rm obs}$ is the total number of available observations. Such complexity is given only by that of the localization algorithm when all observations available are used ($L = N_{\rm obs}$), whereas it also depends on the complexity of feature evaluation and observation selection when a subset of the available observations is used.

The estimation of the target position via the LS algorithm based on range measurements is an NP-hard problem with an exponential complexity on the number of observations $\mathcal{O}(N^m)$ [56]. In the following, $\mathcal{C}_\ell(N)$ denotes the complexity of the localization algorithm as a function of the number N of processed observations, which is $N = L$ with selection of representative observations and $N = N_{\rm obs}$ without selection. Therefore, the complexity for target localization without ($L = N_{\rm obs}$) and with ($L < N_{\rm obs}$) subset selection of representative observations is given by

$$\mathcal{C}(L, N_{\rm obs}) = \begin{cases} \mathcal{C}_\ell(N_{\rm obs}), & L = N_{\rm obs} \\ \mathcal{C}_\ell(L) + \mathcal{C}_{\rm f}(N_{\rm obs}) + \mathcal{C}_{\rm s}(N_{\rm obs}), & L < N_{\rm obs} \end{cases} \tag{10}$$

where $\mathcal{C}_{\rm f}(N_{\rm obs})$ is the complexity of feature evaluation, and $\mathcal{C}_{\rm s}(N_{\rm obs})$ is the complexity of the sorting algorithm based on feature $h(\mathcal{P})$. The term $\mathcal{C}_{\rm s}(N_{\rm obs})$ depends on the sorting algorithm used and is asymptotically quadratic in a worst-case analysis $\mathcal{C}_{\rm s}(N) = \mathcal{O}(N^2)$ [57]. When the term $\mathcal{C}_{\rm f}(N_{\rm obs})$ is a linear function with the number of observations, i.e., $\mathcal{O}(N_{\rm obs})$, the comparison between the computational complexity of localization, with and without observation selection, depends on the complexity of the localization algorithm $\mathcal{C}_\ell(N)$. For example, $\mathcal{C}_\ell(N_{\rm obs}) = \mathcal{O}(N_{\rm obs}^m)$ in the case of a localization algorithm with complexity exponential on the number of observations. In such a case, the selection of representative observations enables significant savings in complexity with $m \geq 2$. A typical value for algorithms operating matrix inversion is $m = 3$.

[7]The specific algorithm for localization is not the main focus of this paper.

IV. Observation Selection Methods

We now introduce blind and low-complexity techniques that exploit diversity and provide selection of observations to alleviate harsh propagation impairments and improve localization performance. The choice of the feature is crucial for the sensor radar's ability to select observations that are representative for target location inference. Therefore, such a choice has to be based on the relation between the feature $h(r_{ij})$ and the range error $e_{ij} = c|\hat{\tau}_{ij}(\mathbf{p}) - \tau_{ij}(\mathbf{p})|$. Consider a decision vector $\overline{\boldsymbol{\epsilon}}_{ij} = [\overline{\epsilon}_{ij}^{(0)}, \overline{\epsilon}_{ij}^{(1)}, \ldots, \overline{\epsilon}_{ij}^{(N_\mathrm{b}-1)}]$ of N_b signal indicator samples for the pair $(i,j) \in \mathcal{P}$ (e.g., with an energy detector (ED), $\overline{\epsilon}_{ij}^{(q)}$ is related to the energy of samples within the qth time interval), then $h(r_{ij}) = h(\overline{\boldsymbol{\epsilon}}_{ij})$. Since the range error depends on the true TOA, the ideal selection would be based on the centrality of $\overline{\epsilon}_{ij}^{(q)}$ distribution with respect to $\tau_{ij}(\mathbf{p})$. Unfortunately, the true TOA is not known in a blind context. We now consider features related to the amplitude and temporal distribution of the decision vector $\overline{\boldsymbol{\epsilon}}_{ij}$ for selecting the observations that are most likely representative of the target (i.e., less affected by multipath, noise, and obstruction loss).

To evaluate the temporal dispersion of $\overline{\boldsymbol{\epsilon}}_{ij}$ over the observation time, we first normalize the qth element (with $q = 0, 1, \ldots, N_\mathrm{b} - 1$), within the each decision vector, as

$$f_{ij}(q) = \frac{\overline{\epsilon}_{ij}^{(q)}}{\sum_{k=0}^{N_\mathrm{b}-1} \overline{\epsilon}_{ij}^{(k)}} \tag{11}$$

where $f_{ij}(q)$ represents the sampling probability that the true TOA belongs to the qth time interval given the vector $\overline{\boldsymbol{\epsilon}}_{ij}$.[8] Define the cumulative distribution function, the first moment, and the nth central moment of $f_{ij}(q)$, respectively, as

$$F_{ij}(x) = \sum_{q \le x} f_{ij}(q) \tag{12}$$

$$\overline{\mu}_{ij} = \sum_{q=0}^{N_\mathrm{b}-1} q f_{ij}(q) \tag{13}$$

$$\mu_{ij}^{(n)} = \sum_{q=0}^{N_\mathrm{b}-1} (q - \overline{\mu}_{ij})^n f_{ij}(q). \tag{14}$$

From (12)–(14), the temporal dispersion of the signal indicator samples can be evaluated by considering variance σ_{ij}^2, interquartile range IQR_{ij}, kurtosis κ_{ij}, and skewness χ_{ij}, which are, respectively, given by

$$\sigma_{ij}^2 = \mu_{ij}^{(2)} \tag{15}$$

$$\mathsf{IQR}_{ij} = F_{ij}^{-1}(0.75) - F_{ij}^{-1}(0.25) \tag{16}$$

$$\kappa_{ij} = \frac{\mu_{ij}^{(4)}}{\left(\mu_{ij}^{(2)}\right)^2} \tag{17}$$

$$\chi_{ij} = \frac{\mu_{ij}^{(3)}}{\left(\sqrt{\mu_{ij}^{(2)}}\right)^3}. \tag{18}$$

To evaluate the amplitude dispersion of $\overline{\boldsymbol{\epsilon}}_{ij}$, consider the maximum value M_{ij}, sample variance s_{ij}^2, sample range r_{ij}, and sample skewness c_{ij}, which are, respectively, given by

$$\mathsf{M}_{ij} = \max_q \overline{\epsilon}_{ij}^{(q)} \tag{19}$$

$$\mathsf{s}_{ij}^2 = \frac{1}{N_\mathrm{b}} \sum_{q=0}^{N_\mathrm{b}-1} \left[\overline{\epsilon}_{ij}^{(q)} - \left(\frac{1}{N_\mathrm{b}} \sum_{k=0}^{N_\mathrm{b}-1} \overline{\epsilon}_{ij}^{(k)} \right) \right]^2 \tag{20}$$

$$\mathsf{r}_{ij} = \left| \max_q \overline{\epsilon}_{ij}^{(q)} - \min_q \overline{\epsilon}_{ij}^{(q)} \right| \tag{21}$$

$$\mathsf{c}_{ij} = \frac{\sum_{q=0}^{N_\mathrm{b}-1} \left[\overline{\epsilon}_{ij}^{(q)} - \frac{1}{N_\mathrm{b}} \left(\sum_{k=0}^{N_\mathrm{b}-1} \overline{\epsilon}_{ij}^{(q)} \right) \right]^3}{N_\mathrm{b} \left(\mathsf{s}_{ij}^2 \right)^{\frac{3}{2}}}. \tag{22}$$

The relation between a feature $h(\overline{\boldsymbol{\epsilon}}_{ij}) \in \{\sigma_{ij}^2, \mathsf{IQR}_{ij}, \kappa_{ij}, \chi_{ij}, \mathsf{s}_{ij}^2, \mathsf{M}_{ij}, \mathsf{r}_{ij}, \mathsf{c}_{ij}\}$ and the range error e_{ij} can be evaluated through the correlation $\rho(h(\overline{\boldsymbol{\epsilon}}_{ij}), \mathsf{e}_{ij})$. Such correlation is determined via both the Spearman and the Pearson correlation coefficients, which indicates whether a monotone relation between the two variables exists [58]. Specifically, the Pearson correlation coefficient for N observations of two variables x and y is given by

$$\rho(x,y) = \frac{\sum_{i=1}^{N} (x_i - \overline{x})(y_i - \overline{y})}{\sqrt{\sum_{i=1}^{N} (x_i - \overline{x})^2} \sqrt{\sum_{j=1}^{N} (y_j - \overline{y})^2}} \tag{23}$$

where x_i and y_i, with $i = 1, \ldots, N$, are observations of x and y, respectively, and $\overline{x}$ and $\overline{y}$ are the average values of the observation sample $\{x_i\}_{i=1}^N$ and $\{y_i\}_{i=1}^N$, respectively. The Spearman correlation coefficient is determined similarly to (23) by using the ranked variables in place of the original ones.[9] Both correlation coefficients take values in $[-1,1]$, where the value $\rho(h(\overline{\boldsymbol{\epsilon}}_{ij}), \mathsf{e}_{ij}) = 0$ indicates that the two variables are uncorrelated, whereas positive or negative values indicate that any monotone relation between the two variables is nondecreasing or nonincreasing, respectively. The statistical significance of such correlation coefficients can be tested based on the sample size and the resulting correlation values providing a p-value, where p represents the probability of obtaining the same correlation coefficient with two independent variables [59].

Consider, for example, the cases $h(\overline{\boldsymbol{\epsilon}}_{ij}) = \sigma_{ij}^2$, $h(\overline{\boldsymbol{\epsilon}}_{ij}) = \chi_{ij}$, and $h(\overline{\boldsymbol{\epsilon}}_{ij}) = \mathsf{c}_{ij}$. Specifically, low or high values of the variance σ_{ij}^2 are obtained with narrow or wide sampling distribution of the time interval containing the true TOA, respectively. Therefore, lower values of σ_{ij}^2 are expected for large values of SNR corresponding to smaller range errors. Differently, positive or negative values of skewness χ_{ij} are obtained when the sampling distribution is right-side or left-side tailed, respectively. In particular, positive values are due to the shape of the channel impulse response, whose right-side tail is given by the delay spread of the channel. The channel impulse response guides the shape of $f_{ij}(q)$ for large SNR values, whereas it has a lower impact for

[8] Note that, in the absence of prior knowledge, we consider the true TOA included in the maximum element of $\overline{\boldsymbol{\epsilon}}_{ij}$ with highest probability.

[9] Ranking is performed by sorting the observations in ascending order and associating them with the corresponding ordinal number.

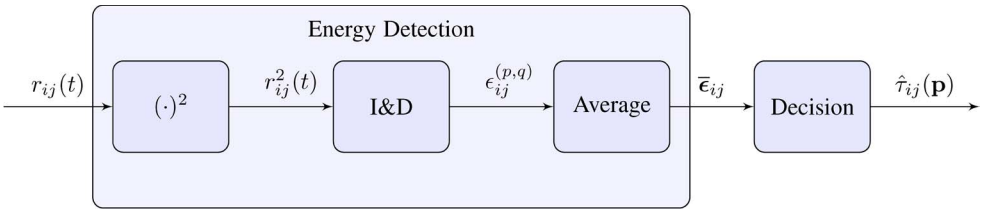

Fig. 3. TOA estimation based on energy detection for the radar $(i,j) \in \mathcal{P}$.

small SNR values. Therefore, higher values of χ_{ij} are expected for smaller range errors. Finally, low or high values of sample skewness are obtained when there are many or few elements with large values within the decision vector $\overline{\boldsymbol{\epsilon}}_{ij}$, respectively. Large-value indicator samples are more likely to be associated with the target for large SNR values, when the energy due to the target is easily discernible from the noise floor. Therefore, higher values of c_{ij} are expected for smaller range errors.

The observations $\hat{\boldsymbol{\tau}}_{\mathcal{P}}(\mathbf{p})$ are sorted based on the features $h(\overline{\boldsymbol{\epsilon}}_{\mathcal{P}})$ in increasing or decreasing order, depending on whether the relation between $h(\overline{\boldsymbol{\epsilon}}_{ij})$ and e_{ij} is monotonically nonincreasing or nondecreasing, respectively.[10] Then, the subset $\hat{\boldsymbol{\tau}}_{\mathcal{P}_{\mathrm{sel}}}(\mathbf{p})$ of $L = |\mathcal{P}_{\mathrm{sel}}| \leq N_{\mathrm{obs}}$ selected observations is composed by the first L sorted observations and further processed by the localization algorithm.

From (10), the comparison between the computational complexity of localization with and without observation selection depends on the complexity of the localization algorithm $\mathcal{C}_\ell(N)$. Note that the term $\mathcal{C}_{\mathrm{f}}(N_{\mathrm{obs}})$ is a linear function with the number of observations $\mathcal{O}(N_{\mathrm{obs}})$ for all the aforementioned features, except for the IQR_{ij} that requires function inversion. Therefore, the selection of representative observations enables significant savings in complexity when $m \geq 2$.

The extraction of the aforementioned features will be detailed in the following for a case of wide usage based on sub-Nyquist processing with energy detection.

V. Observation Processing

We now describe the signal preprocessing techniques and TOA estimation.

A. Prefiltering and Clutter Removal

The out-of-band noise can be mitigated by means of a bandpass zonal filter (BPZF), which consists of a bandpass filter having the same center frequency and bandwidth of the transmitted signal. The output of the BPZF, corresponding to the transmission of N_{p} pulses, is given by

$$\tilde{v}_{ij}(t) = \sum_{p=0}^{N_{\mathrm{p}}-1} \sum_{l=0}^{L_{\mathrm{p}}-1} \alpha_{ij}^{(l)} s\left(t - pT_{\mathrm{g}} - \tau_{ij}^{(l)}\right) + w_{ij}(t) \quad (24)$$

where $s(t)$ is the output of the BPZF corresponding to a single pulse at its input, L_{p} is the number of received multipath components due to target backscattering (with the lth component having gain $\alpha_{ij}^{(l)}$ and delay $\tau_{ij}^{(l)}$), and $T_{\mathrm{g}} \triangleq 1/\mathsf{PRF}$. The term $w_{ij}(t)$ includes the filtered components of noise and clutter.

There are various techniques for clutter removal, based on the operation environment. In case of static clutter, two classical techniques are the empty-room technique and the frame-to-frame technique. The empty-room technique consists of a setup phase where a signal, namely, reference signal, is received and recorded at each radar in the absence of a target object [60]. Such a reference signal is recorded offline from a high number of transmitted pulses, and therefore, it includes the time-invariant clutter. Then, the reference signal is subtracted from the signal received in the presence of target objects to mitigate static clutter. The frame-to-frame technique exploits the amplitude and phase variations of backscattered signals due to the target mobility for discerning the time-invariant clutter from the moving target [42]. In the case of nonstatic clutter, both clutter removal techniques present a residual clutter in the waveforms at the input of the TOA estimator.

B. TOA and Position Estimation

A variety of TOA estimators is present in the literature; those based on energy detection received attention because they are based on noncoherent signal reception and sub-Nyquist sampling. In particular, with energy detection, the TOA estimates are determined based on energy values collected in time intervals (energy bins) [31].

The signal at the input of the TOA estimator, after prefiltering and clutter removal, is given by

$$r_{ij}(t) = \sum_{p=0}^{N_{\mathrm{p}}-1} \sum_{l=0}^{L_{\mathrm{p}}-1} \alpha_{ij}^{(l)} s\left(t - pT_{\mathrm{g}} - \tau_{ij}^{(l)}\right) + n_{ij}(t) \quad (25)$$

where $n_{ij}(t)$ includes the filtered noise and the residual clutter.

Fig. 3 shows the TOA estimator based on energy detection and decision by comparing each energy bin averaged over multiple received pulses with a threshold. The TOA estimator uses a temporal part of the signal $r_{ij}(t)$ with duration T_{g}, including only one received pulse to avoid ambiguous TOA estimations, and then, it accumulates over N_{p} transmitted pulses. The goal is to determine $\hat{d}_{ij}(\mathbf{p})$ from the estimate $\hat{\tau}_{ij}^{(1)}$.[11] In the absence of prior information, we consider the true $\tau_{ij}(\mathbf{p})$ uniformly

[10] The features $h(\overline{\boldsymbol{\epsilon}}_{\mathcal{P}})$ are calculated based on the vector $\overline{\boldsymbol{\epsilon}}_{\mathcal{P}}$, that contains all the decision vectors $\overline{\boldsymbol{\epsilon}}_{ij}$ with $(i,j) \in \mathcal{P}$.

[11] Note that after perfect clutter removal, multipath propagation in (25) accounts for the paths scattered by the target, and these paths arrive at the receiver after reflections.

distributed in the interval $[0, T_{\rm a}]$, where the maximum possible delay $T_{\rm a}$ depends on the propagation environment. The PRF is chosen to satisfy $T_{\rm g} > T_{\rm a}$.

The ED is composed of a square-law device followed by an integrate and dump (I&D) block with dwell time $T_{\rm dwell}$. Then, the ED provides a vector of $N_{\rm b} = \lfloor T_{\rm g}/T_{\rm dwell} \rfloor$ energy bins. The qth energy bin for the pth received waveform of the radar (i, j) is given by[12]

$$\epsilon_{ij}^{(p,q)} = \int_{qT_{\rm dwell}+pT_{\rm g}}^{(q+1)T_{\rm dwell}+pT_{\rm g}} r_{ij}^2(t)\, dt \tag{26}$$

with $p = 0, 1, \ldots, N_{\rm p} - 1$, and $q = 0, 1, \ldots, N_{\rm b} - 1$.

A decision vector based on energy bins (namely, the energy vector) is obtained as $\overline{\boldsymbol{\epsilon}}_{ij} = [\bar{\epsilon}_{ij}^{(0)}, \bar{\epsilon}_{ij}^{(1)}, \ldots, \bar{\epsilon}_{ij}^{(N_{\rm b}-1)}]$, where the qth element $\bar{\epsilon}_{ij}^{(q)}$ is determined, for example, by averaging over the $N_{\rm p}$ received signals [31], i.e.,

$$\bar{\epsilon}_{ij}^{(q)} = \frac{1}{N_{\rm p}} \sum_{p=0}^{N_{\rm p}-1} \epsilon_{ij}^{(p,q)}. \tag{27}$$

The TOA estimation is made by comparing each element $\bar{\epsilon}_{ij}^{(q)}$ with a threshold ξ_{ij}. From such a comparison, the decision is taken on the bin inside which the true TOA is detected. The choice of the threshold ξ_{ij} is crucial for the TOA estimation, as well as for the level of misdetection and false alarms. In this paper, the threshold is designed based on a constant false-alarm approach, i.e., the threshold ξ_{ij} is chosen to obtain a constant probability of the event that an only-noise energy bin is above the threshold.[13] For the radar $(i, j) \in \mathcal{P}$ and target at $\mathbf{p}$, the estimated TOA $\hat{\tau}_{ij}(\mathbf{p})$ is chosen as the central value of the corresponding dwell interval for the first element of the energy vector above the threshold ξ_{ij}.

The amplitude and temporal distributions of the elements $\bar{\epsilon}_{ij}^{(q)}$ depend on the true TOA $\tau_{ij}(\mathbf{p})$ and the received SNR $\gamma_{ij}(\mathbf{p})$, which are affected by propagation conditions (i.e., noise, path loss, and obstruction loss). Fig. 4 shows three examples of energy vectors $\bar{\epsilon}_{ij}^{(q)}$ as a function of q for different signal path lengths and total thickness of the crossed walls. Note that the true TOA $\tau_{ij}(\mathbf{p})$, which is dependent on both signal path length and obstructions, guides the centrality of distribution of $\bar{\epsilon}_{ij}^{(q)}$, whereas the SNR, which is dependent on path loss and obstruction loss, guides the amplitude and temporal dispersion of $\bar{\epsilon}_{ij}^{(q)}$. Decisions provided by comparison with a threshold in the case of disperse distribution of energy bins are more vulnerable to nonrepresentative elements of the observation vector. Hence, $\hat{\tau}_{ij}(\mathbf{p})$ is most likely due to a nonrepresentative observation of the target when the values $\bar{\epsilon}_{ij}^{(q)}$ have a flat distribution with values close to the noise floor.

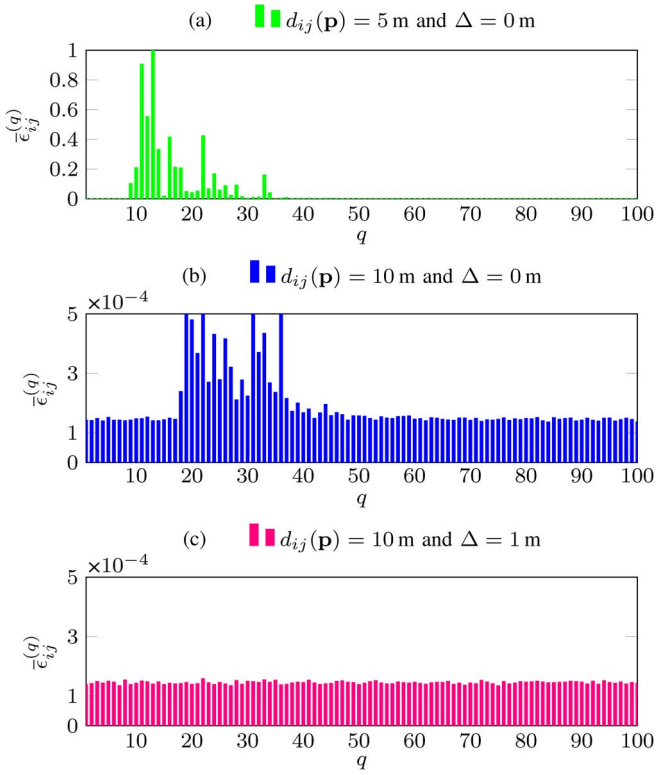

Fig. 4. Energy vectors for different values of signal path-length $d_{ij}(\mathbf{p})$ and total wall thickness Δ. Energy values are normalized to the maximum of the vector in (a). Results are obtained with an ED setting and channel model used in the case study (see Section VI).

VI. Case Study

We now present a case study for a network of UWB sensor radars that operates in an indoor environment and that exploits the selection of representative observations. The performance metrics, the operation environment, the signal processing techniques, and the numerical results are described in the following subsections.

A. Performance Metrics

The localization performance is evaluated in terms of localization error and localization error outage (LEO). The localization error is defined as the Euclidean distance between the estimated position $\hat{\mathbf{p}}$ and the true position $\mathbf{p}$ of the target, as given by

$$e(\mathbf{p}) = \|\hat{\mathbf{p}} - \mathbf{p}\|. \tag{28}$$

The LEO is defined as the probability that the localization error is above a maximum tolerable value $e_{\rm th}$, as given by

$$P_{\rm LEO} = \mathbb{P}\{e(\mathbf{p}) > e_{\rm th}\} = \mathbb{E}_{\mathbf{p}}\left\{1_{(e_{\rm th},+\infty)}\{\|\hat{\mathbf{p}} - \mathbf{p}\|\}\right\} \tag{29}$$

where $1_{\mathcal{B}}\{x\} \triangleq 1$ if $x \in \mathcal{B}$ and 0, otherwise.[14]

[12] Remember that the collection of energy from successive received waveforms increases the performance of the TOA estimator.

[13] We refer to only-noise bins as those with energy due only to noise. Note that this threshold represents an optimal solution in additive white Gaussian noise channels. Alternatively, in [61], a simple criterion to determine a threshold based on the evaluation of early detection probability and noise power knowledge is proposed for multipath channels.

[14] $\mathbb{P}\{\cdot\}$ denotes probability and $\mathbb{E}_{\rm x}\{\cdot\}$ denotes the statistical expectation averaged over the random variable (RV) x.

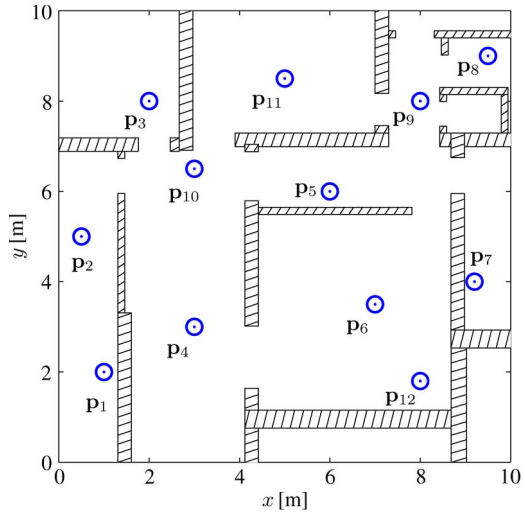

Fig. 5. Operation environment with sensor radars and walls. Sensor position coordinates are $\mathbf{p}_1 = (1, 2)$, $\mathbf{p}_2 = (0.5, 5)$, $\mathbf{p}_3 = (2, 8)$, $\mathbf{p}_4 = (3, 3)$, $\mathbf{p}_5 = (6, 6)$, $\mathbf{p}_6 = (7, 3.5)$, $\mathbf{p}_7 = (9.2, 4)$, $\mathbf{p}_8 = (9.5, 8)$, $\mathbf{p}_9 = (8, 8)$, $\mathbf{p}_{10} = (3, 6.5)$, $\mathbf{p}_{11} = (5, 8.5)$, and $\mathbf{p}_{12} = (8, 1.8)$, in meters.

B. Operation Environment

1) Scenario: Fig. 5 shows the operation environment of 10 m $\times$ 10 m with walls, in which $N_{\mathrm{S}} = |\mathcal{S}| = 12$ UWB sensors are placed. Results are compared with those obtained in the absence of walls. In the operation environment, the maximum TOA value is $T_{\mathrm{a}} = 94.2$ ns (corresponding to the TOA of a signal traveling over a distance of twice a diagonal line). The network of sensor radars varies its configuration during the localization process. Specifically, we consider $N_{\mathrm{S}} - 1$ multistatic configurations with a single transmitter and multiple receivers. At the nth configuration, there is one transmitter at $\mathbf{p}_n$ and the $N_{\mathrm{S}} - n$ receivers in positions $\{\mathbf{p}_{n+1}, \mathbf{p}_{n+2}, \ldots, \mathbf{p}_{N_{\mathrm{S}}}\}$. In reciprocal channels, the choice of these multistatic configurations ensures diverse propagation paths for received signals $r_{ij}(t)$ with a single observation per sensor pair. The total number of observations is $N_{\mathrm{obs}} = N_{\mathrm{S}}(N_{\mathrm{S}} - 1)/2$ (i.e., $N_{\mathrm{obs}} = 66$ for $N_{\mathrm{S}} = 12$).

The impulse radio UWB sensor radars transmit a sequence of root-raised-cosine pulses compliant with the European lower band with $\mathsf{PRF} = 5$ MHz. The antennas are omnidirectional, and the one-sided noise PSD is $N_0 = -200$ dBW/Hz (e.g., noise figure $F = 6$ dB and antenna noise temperature 290 K).

2) Multipath and Clutter: Multipath propagation for the direct signal (from transmitter to target) and backscattered signal (from target to receiver) are modeled according to IEEE 802.15.4a [54] for a residential LOS environment. The NLOS conditions caused by walls generate obstruction loss and excess delay, which are taken into account as described in Section II-B. For each TOA estimation, the presence of 100 clutter objects uniformly distributed in the operation environment is considered. Such clutter is static, with RCS for each object obtained as a realization of a Swerling type-V RCS (i.e., a Chi-squared RV with four degrees of freedom).

3) Target: A Swerling type-III RCS Σ is considered for the target, which models a human body with random RCS distributed as a Chi-squared RV with four degrees of freedom, constant during a scan (i.e., the transmission of N_{p} pulses necessary for the TOA estimation process), and independent from scan to scan [7]. The average RCS is $\mathbb{E}\{\Sigma\} = 1$ m^2, which is typical for the human body [62].

C. Signal Processing and Localization Algorithm

The energy vector $\overline{\boldsymbol{\epsilon}}_{ij}$ for each radar $(i, j) \in \mathcal{P}_{\mathrm{sel}}$ is obtained via an ED with dwell time $T_{\mathrm{dwell}} = 2$ ns and observation time $T_{\mathrm{g}} = 200$ ns. Then, a TOA estimate $\hat{\tau}_{ij}(\mathbf{p})$ is determined through comparison with a threshold ξ_{ij}, which is chosen to obtain a constant probability of the event that an only-noise energy bin is above the threshold. Therefore, $\mathbb{P}\{\overline{\epsilon} > \xi_{ij}\} = 10^{-3}$ when $\overline{\epsilon}$ is an only-noise bin (e.g., corresponding to an absence of the target). The static clutter is mitigated via an empty-room algorithm with reference signal obtained by averaging 100 received waveforms in an absence of the target [42].

We evaluate the performance of the sensor radar network when L observations are selected based on the eight different features presented in Section V, i.e., $h(\overline{\boldsymbol{\epsilon}}_{ij}) \in \{\sigma^2_{ij}, \mathsf{IQR}_{ij}, \kappa_{ij}, \chi_{ij}, \mathsf{s}^2_{ij}, \mathsf{M}_{ij}, \mathsf{r}_{ij}, \mathsf{c}_{ij}\}$ for $(i, j) \in \mathcal{P}_{\mathrm{sel}}$. To evaluate the benefits offered by selecting representative observations using the proposed features, a case in which L observations are randomly chosen is also presented for comparison. In addition, a nonblind case is presented as a benchmark, where the L energy vectors are chosen as those leading to the minimum range errors by using $h(\overline{\boldsymbol{\epsilon}}_{ij}) = \mathsf{e}_{ij} = c|\hat{\tau}_{ij}(\mathbf{p}) - \tau_{ij}(\mathbf{p})|$. There, localization is performed based on the selected observations for 1000 target positions uniformly distributed in the environment in Fig. 5 with and without walls.

D. Numerical Results

We now present results related to the choice of observation selection features and to the localization accuracy.

1) Observation Selection Features: Figs. 6 and 7 show the variance σ_{ij} and kurtosis κ_{ij}, respectively, for two bistatic radars in the network (transmitter indexed by $i = 6$ and receiver indexed by $j = 10$ or 12). One thousand target positions uniformly distributed in the environment with walls are considered. It can be observed how the feature varies with the signal propagation conditions (i.e., target in LOS or NLOS conditions with both transmitter and receiver). In particular, Fig. 6 shows that high values of variance σ_{ij} are obtained when the target is in LOS conditions with both transmitter and receiver [i.e., Fig. 6(b)] or in light NLOS conditions [i.e., Fig. 6(a)].[15] Fig. 7 shows that high values of kurtosis can be obtained not only in LOS and light NLOS conditions but under heavy NLOS conditions as well (e.g., for targets in the bottom-right corner of the environment). These results indicate that using the variance as feature enables a more accurate selection of representative observations than using the kurtosis. Therefore, we expect a correlation $|\rho(\sigma_{ij}, \mathsf{e}_{ij})|$ higher than $|\rho(\kappa_{ij}, \mathsf{e}_{ij})|$.

To understand the ability of the features proposed in Section IV to indicate representative observations, Fig. 8 shows

[15]We refer to light or heavy NLOS conditions when one or more walls are present in the signal propagation path, respectively.

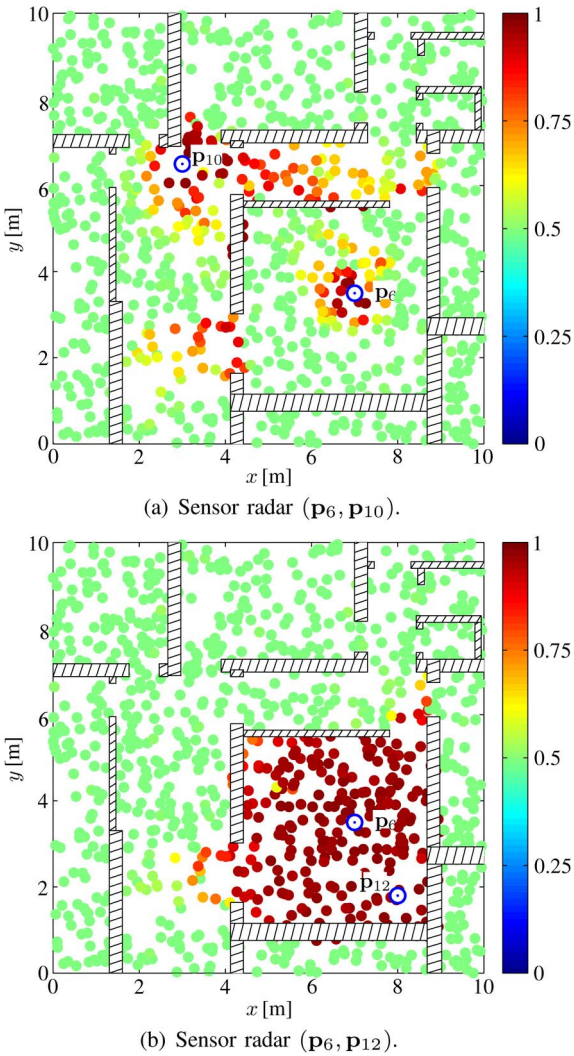

(a) Sensor radar $(\mathbf{p}_6, \mathbf{p}_{10})$.

(b) Sensor radar $(\mathbf{p}_6, \mathbf{p}_{12})$.

Fig. 6. Color map of variance σ_{ij}^2 with $i = 6$ and $j = 10, 12$, for 1000 target positions uniformly distributed in the environment. The value of σ_{ij}^2 is normalized to the maximum value in the environment.

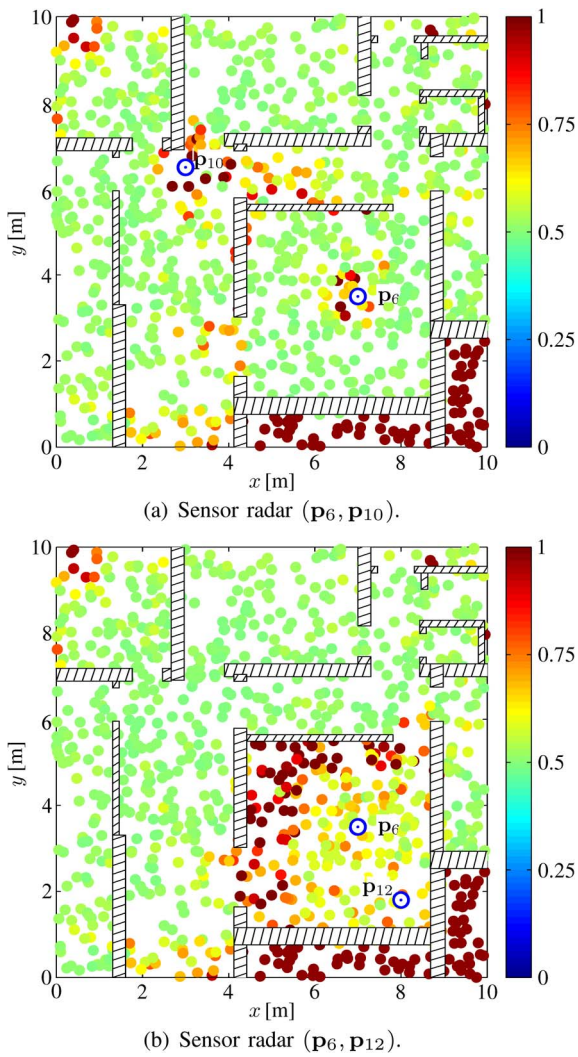

(a) Sensor radar $(\mathbf{p}_6, \mathbf{p}_{10})$.

(b) Sensor radar $(\mathbf{p}_6, \mathbf{p}_{12})$.

Fig. 7. Color map of kurtosis κ_{ij}^2 with $i = 6$ and $j = 10, 12$, for 1000 target positions uniformly distributed in the environment. The value of κ_{ij}^2 is normalized to the maximum value in the environment.

the Spearman and Pearson correlations between each feature $h(\overline{\boldsymbol{\epsilon}}_{ij})$ and the range error e_{ij}. The nonblind case with $h(\overline{\boldsymbol{\epsilon}}_{ij}) = \mathsf{e}_{ij}$ used as a benchmark is also presented. Correlation is obtained by considering a data set of $1000 \times N_{\text{obs}}$ energy vectors (i.e., one energy vector per transmitter–receiver pair, for each of the 1000 uniformly distributed target positions). We verified that the p-value is lower than 10^{-5} for all the features according to both Spearman and Pearson's correlations, which indicates that the correlation is statistically significant [59]. Specifically, low or high values of $|\rho(h(\overline{\boldsymbol{\epsilon}}_{ij}), \mathsf{e}_{ij})|$ indicate a weak or strong capability of selecting representative observations using the feature $h(\overline{\boldsymbol{\epsilon}}_{ij})$, respectively. The positive or negative sign of $\rho(h(\overline{\boldsymbol{\epsilon}}_{ij}), \mathsf{e}_{ij})$ indicates that the lower values of $h(\overline{\boldsymbol{\epsilon}}_{ij})$ are most likely to provide smaller or larger range errors, respectively. Therefore, the subset of representative observations leading to the lower or higher values of $h(\overline{\boldsymbol{\epsilon}}_{ij})$ is selected if the sign of $\rho(h(\overline{\boldsymbol{\epsilon}}_{ij}), \mathsf{e}_{ij})$ is positive or negative, respectively. Note that the correlation for the feature $h(\overline{\boldsymbol{\epsilon}}_{ij}) = \sigma_{ij}^2$ is 0.38 with Pearson's method and 0.44 with Spearman's method; the correlation for the feature $h(\overline{\boldsymbol{\epsilon}}_{ij}) = \chi_{ij}$ is -0.71 with Pearson's method and -0.64 with Spearman's method; and the correlation for the feature $h(\overline{\boldsymbol{\epsilon}}_{ij}) = \mathsf{c}_{ij}$ is -0.71 with Pearson's method and -0.90 with Spearman's method. Therefore, the selection of representative observations leading to the lower variance, the higher skewness, or high sample skewness most likely provides small range errors.

Based on these results, we evaluate the effects of observation selection on the localization performance for these three features, which present large values of correlation together with linear computational complexity.

2) Localization Performance: Fig. 9 shows the LEO at $e_{\text{th}} = 1$ m as a function of the number of selected observations L for $h(\overline{\boldsymbol{\epsilon}}_{ij}) = \sigma_{ij}^2, \kappa_{ij}$, and M_{ij}. To better understand the importance of the observation selection features on localization accuracy, the results are also obtained by considering a random selection of the L observations. The nonblind case $h(\overline{\boldsymbol{\epsilon}}_{ij}) = \mathsf{e}_{ij}$ serves as a benchmark. In the absence of walls (LOS conditions), all selection features provide a LEO that decreases with the number of selected observations. This is expected from the absence of obstruction loss and excess delay. However, note

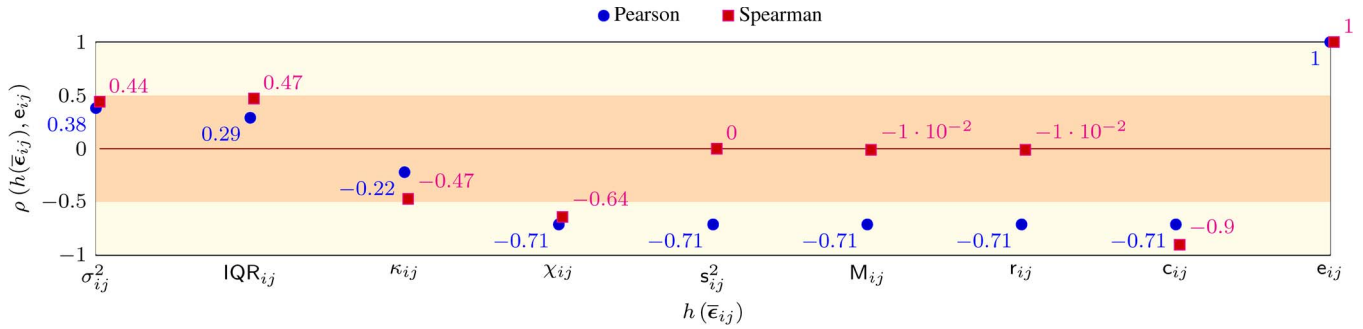

Fig. 8. Pearson and Spearman correlation coefficients between each considered feature and the range error. Green and red regions represent index values of either strong or weak correlation, respectively. The red line represents the case of uncorrelation between the two variables.

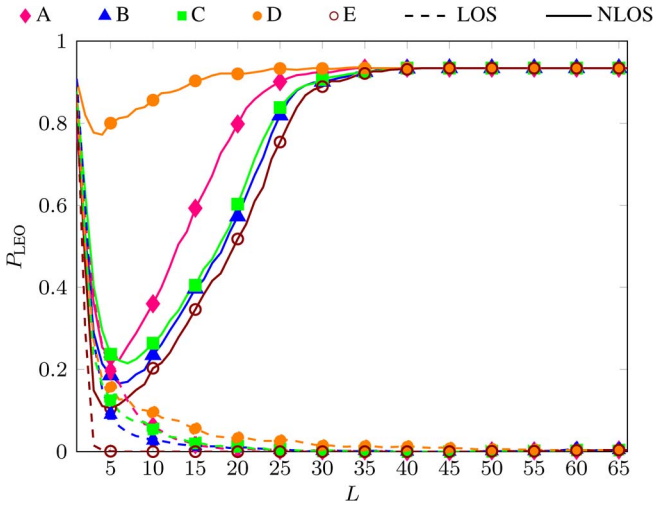

Fig. 9. LEO as a function of $L = 1, 2, \ldots, N_{\mathrm{obs}}$ for $e_{\mathrm{th}} = 1$ m, with (solid) and without (dashed) walls, for the cases (A)$h(\overline{\epsilon}_{ij}) = \sigma^2_{ij}$, (B)$h(\overline{\epsilon}_{ij}) = \kappa_{ij}$, and (C)$h(\overline{\epsilon}_{ij}) = \mathsf{M}_{ij}$. Case (D) represents the random choice of L observations. Case (E) refers to the nonblind case $h(\overline{\epsilon}_{ij}) = \mathsf{e}_{ij}$.

that $L = 5$ observations, even randomly chosen, are sufficient to have a localization error $e_{\mathrm{p}}(\mathbf{p}) < 1$ m in 80% of cases despite that only $L = 5$ TOA estimates out of 66 are processed. This significantly reduces localization complexity, which is a quadratic function of the number of estimates that are processed. The worse performance levels for $L < 5$ are mainly due to ambiguities (e.g., ghost targets [7]) given by the intersection of L isorange contours (ellipses in two dimensions) leading to more than a single point in the absence of prior information (e.g., information on the environment). In the presence of walls (NLOS conditions), the LEO presents a minimum for all the selection features with $L = 5$ or 6. Here, the effect of selection is clear since in the case with $L = 5$, the localization error is $e_{\mathrm{p}}(\mathbf{p}) < 1$ m in 20% of cases for random observation choice and in 77%, 80%, and 76% of cases for $h(\overline{\epsilon}_{ij}) = \sigma^2_{ij}, \chi_{ij}$, and c_{ij}, respectively. Note also that the localization error is $e_{\mathrm{p}}(\mathbf{p}) <$ 1 m in only 7% of cases when no selection is performed (i.e., all the $L = N_{\mathrm{obs}} = 66$ observations are processed). Therefore, the performance improvement offered by the proposed method for this selection of representative observations is remarkable.

Fig. 10 shows the LEO as a function of e_{th} for $L = 5$ selected observations using the features considered in Fig. 9. In the absence of walls [see Fig. 10(a)], the localization error in 80% of cases is below 0.08 m for the nonblind case $h(\overline{\epsilon}_{ij}) = \mathsf{e}_{ij}$, 0.98 m for $h(\overline{\epsilon}_{ij}) = \sigma^2_{ij}$, 0.72 m for $h(\overline{\epsilon}_{ij}) = \chi_{ij}$, 0.74 m for $h(\overline{\epsilon}_{ij}) = \mathsf{c}_{ij}$, and 0.84 m for the random observation selection. Note that the random choice shows similar performance to the other selection techniques in the absence of obstructions. This is due to the fact that range measurements almost have the same representativeness in the absence of obstruction loss and excess delay. In the presence of walls [see Fig. 10(b)], the localization error in 80% of cases is below 0.42 m for the nonblind case $h(\overline{\epsilon}_{ij}) = \mathsf{e}_{ij}$, 1.1 m for $h(\overline{\epsilon}_{ij}) = \sigma^2_{ij}$, 0.96 m for $h(\overline{\epsilon}_{ij}) = \mathsf{k}_{ij}$, and 1 m for $h(\overline{\epsilon}_{ij}) = \mathsf{c}_{ij}$. Note that the localization error is above 3 m in 49% of cases when the subset of observations is randomly selected. This highlights that, together with complexity reduction, the processing of a small subset of properly selected representative observations significantly improves the localization performance. It is remarkable that proper observation selection can provide localization performance close to that in the absence of walls.

VII. Conclusion

The intrinsic properties of sensor radar networks and the representativeness of their observations determine the localization accuracy, particularly in harsh propagation environments. Blind methods for observation selection have been proposed based on features extracted from the received waveforms. Our methodology inspects the network setting, propagation environment, waveform processing, observation selection, and localization algorithm in the absence of prior information. It shows the importance of selecting representative observations for localization accuracy in non-light-of-sight conditions, particularly by adopting the appropriate selection features. In fact, in addition to a reduction in the overall localization complexity, observation selection significantly improves the performance in the presence of obstacles. The localization performance of a network of ultra-wideband sensor radars operating in an indoor environment with multipath, clutter, and obstructions has been determined based on the proposed methods for observation selection and signal processing. Results show that, in the presence of obstructions due to walls, the proposed selection methods strongly improve the localization accuracy. For example, the localization error outage at 1 m improves from 93% without

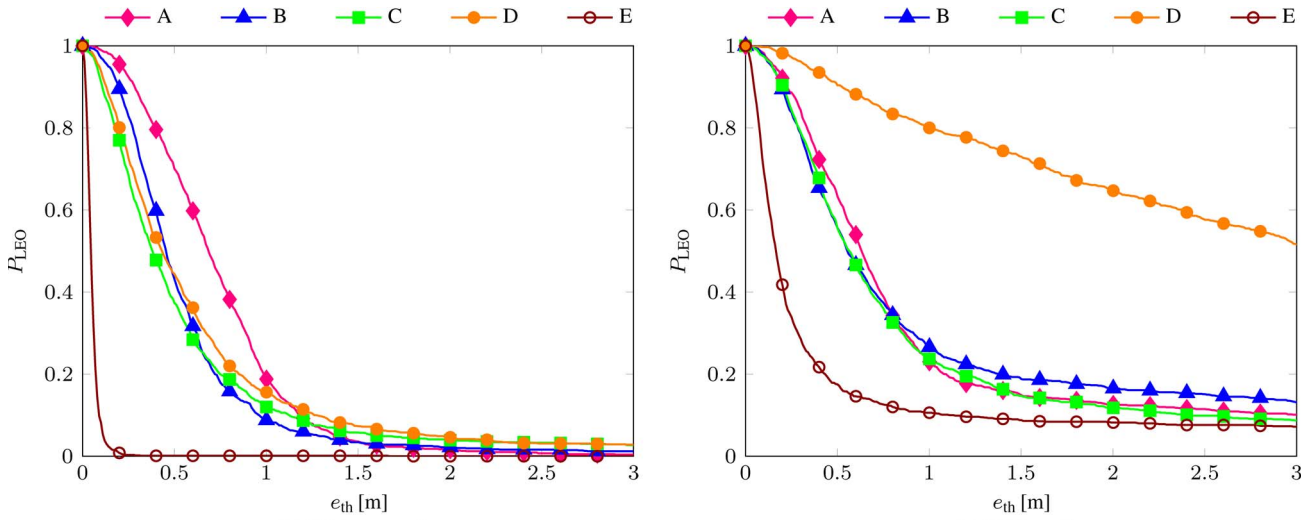

Fig. 10. LEO as a function of e_{th}, with $L = 5$ and $N_{\mathrm{obs}} = 66$, for the cases (A)$h(\overline{\boldsymbol{\epsilon}}_{ij}) = \sigma_{ij}^2$, (B)$h(\overline{\boldsymbol{\epsilon}}_{ij}) = \kappa_{ij}$, (C)$h(\overline{\boldsymbol{\epsilon}}_{ij}) = \mathsf{M}_{ij}$. Case (D) represents the random choice of L observations. Case (E) refers to the nonblind cases, where $h(\overline{\boldsymbol{\epsilon}}_{ij}) = e_{ij}^2$.

observation selection to 23% with the proposed observation selection method.

REFERENCES

[1] M. Z. Win *et al.*, "Network localization and navigation via cooperation," *IEEE Commun. Mag.*, vol. 49, no. 5, pp. 56–62, May 2011.

[2] F. Falcone, P. Colone, and P. Lombardo, "Potentialities and challenges of WiFi-based passive radar," *IEEE Trans. Aerosp. Electron. Syst.*, vol. 27, no. 11, pp. 15–26, Nov. 2012.

[3] F. Colone, P. Falcone, C. Bongioanni, and P. Lombardo, "WiFi-based passive bistatic radar: Data processing schemes and experimental results," *IEEE Trans. Aerosp. Electron. Syst.*, vol. 48, no. 2, pp. 1061–1079, Apr. 2012.

[4] F. Colone, P. Falcone, C. Bongioanni, and P. Lombardo, "UWB ranging accuracy in high and low data rate applications," *IEEE Trans. Microw. Theory Tech.*, vol. 54, no. 4, pp. 1865–1875, Jun. 2006.

[5] R. Martin, J. Velotta, and J. Raque, "Bandwidth efficient cooperative TDOA computation for multicarrier signals of opportunity," *IEEE Trans. Signal Process.*, vol. 57, no. 6, pp. 2311–2322, Jun. 2009.

[6] M. I. Skolnik, "An analysis of bistatic radar," *IEEE Trans. Aerosp. Navig. Electron.*, vol. ANE-8, no. 1, pp. 19–27, Mar. 1961.

[7] M. I. Skolnik, *Radar Handbook*, 2nd ed. New York, NY, USA: McGraw-Hill, 1990.

[8] V. S. Chernyak, *Fundamentals of Multisite Radar Systems: Multistatic Radars and Multistatic Radar Systems*. London, U.K.: CRC, 1998.

[9] *IEEE Standard Radar Definitions*, IEEE Std. 686-1990, Aerosp. Electron. Syst. Soc., Apr. 1990.

[10] A. H. Welsh, *Aspects of Statistical Inference*. Hoboken, NJ, USA: Wiley, 2011.

[11] L. Mucchi, E. D. Re, and T. Landi, "Multi-level environment identification method for impulsive radio systems," in *Proc. IEEE Int. Conf. Ultra-Wideband*, Bologna, Italy, Sep. 2011, pp. 385–389.

[12] P. Closas, C. Fernández-Prades, and J. A. Fernandez-Rubio, "A Bayesian approach to multipath mitigation in GNSS receivers," *IEEE J. Sel. Topics Signal Process.*, vol. 3, no. 4, pp. 695–706, Aug. 2009.

[13] P. Closas and C. Fernández-Prades, "A statistical multipath detector for antenna array based GNSS receivers," *IEEE Trans. Wireless Commun.*, vol. 10, no. 3, pp. 916–929, Mar. 2011.

[14] P. Closas and M. F. Bugallo, "Improving accuracy by iterated multiple particle filtering," *IEEE Signal Process. Lett.*, vol. 19, no. 8, pp. 531–534, Aug. 2012.

[15] H.-C. Wu, Y. Wu, J. C. Principe, and X. Wang, "Robust switching blind equalizer for wireless cognitive receivers," *IEEE Trans. Wireless Commun.*, vol. 7, no. 5, pp. 1461–1465, May 2008.

[16] A. Athalye, V. Savic, M. Bolic, and P. M. Djuric, "Novel semi-passive RFID system for indoor localization," *IEEE Sensors J.*, vol. 13, no. 2, pp. 528–537, Feb. 2013.

[17] E. A. de Reyna and P. M. Djuric, "Indoor localization with range-based measurements and little prior information," *IEEE Sensors J.*, vol. 13, no. 5, pp. 1979–1987, May 2013.

[18] H. Godrich, A. Petropulu, and H. Poor, "Sensor selection in distributed multiple-radar architectures for localization: A knapsack problem formulation," *IEEE Trans. Signal Process.*, vol. 60, no. 1, pp. 247–260, Jan. 2012.

[19] L. Kaplan, "Global node selection for localization in a distributed sensor network," *IEEE Trans. Aerosp. Electron. Syst.*, vol. 42, no. 1, pp. 113–135, Jan. 2006.

[20] L. Kaplan, "Local node selection for localization in a distributed sensor network," *IEEE Trans. Aerosp. Electron. Syst.*, vol. 42, no. 1, pp. 136–146, Jan. 2006.

[21] M. Z. Win and R. A. Scholtz, "Impulse radio: How it works," *IEEE Commun. Lett.*, vol. 2, no. 2, pp. 36–38, Feb. 1998.

[22] M. Z. Win and R. A. Scholtz, "Ultra-wide bandwidth time-hopping spread-spectrum impulse radio for wireless multiple-access communications," *IEEE Trans. Commun.*, vol. 48, no. 4, pp. 679–691, Apr. 2000.

[23] L. Yang and G. B. Giannakis, "Ultra-wideband communications: An idea whose time has come," *IEEE Signal Process. Mag.*, vol. 21, no. 6, pp. 26–54, Nov. 2004.

[24] Y. Shen, S. Mazuelas, and M. Z. Win, "Network navigation: Theory and interpretation," *IEEE J. Sel. Areas Commun.*, vol. 30, no. 9, pp. 1823–1834, Oct. 2012. [Online]. Available: http://arxiv.org/abs/1112.3599

[25] Y. Shen and M. Z. Win, "Fundamental limits of wideband localization—Part I: A general framework," *IEEE Trans. Inf. Theory*, vol. 56, no. 10, pp. 4956–4980, Oct. 2010. [Online]. Available: http://arxiv.org/abs/1006.0888v1

[26] Y. Shen and M. Z. Win, "On the accuracy of localization systems using wideband antenna arrays," *IEEE Trans. Commun.*, vol. 58, no. 1, pp. 270–280, Jan. 2010.

[27] S. Gezici *et al.*, "Localization via ultra-wideband radios: A look at positioning aspects for future sensor networks," *IEEE Signal Process. Mag.*, vol. 22, no. 4, pp. 70–84, Jul. 2005.

[28] R. J. Fontana and S. J. Gunderson, "Ultra-wideband precision asset location system," in *Proc. IEEE Conf. Ultra Wideband Syst. Technol.*, May 2002, pp. 147–150.

[29] S. Gezici and H. V. Poor, "Position estimation via ultra-wide-band signals," *Proc. IEEE*, vol. 97, no. 2, pp. 386–403, Feb. 2009.

[30] A. Giorgetti and M. Chiani, "Time-of-arrival estimation based on information theoretic criteria," *IEEE Trans. Signal Process.*, vol. 61, no. 8, pp. 1869–1879, Apr. 2013.

[31] D. Dardari, A. Conti, U. J. Ferner, A. Giorgetti, and M. Z. Win, "Ranging with ultrawide bandwidth signals in multipath environments," *Proc. IEEE*, vol. 97, no. 2, pp. 404–426, Feb. 2009.

[32] L. Stoica, A. Rabbachin, and I. Oppermann, "A low-complexity noncoherent IR-UWB transceiver architecture with TOA estimation," *IEEE Trans. Microw. Theory Tech.*, vol. 54, no. 4, pp. 1637–1646, Jun. 2006.

[33] D. B. Jourdan, D. Dardari, and M. Z. Win, "Position error bound for UWB localization in dense cluttered environments," *IEEE Trans. Aerosp. Electron. Syst.*, vol. 44, no. 2, pp. 613–628, Apr. 2008.
[34] F. Ahmad and M. G. Amin, "Noncoherent approach to through-the-wall radar localization," *IEEE Trans. Aerosp. Electron. Syst.*, vol. 42, no. 4, pp. 1405–1419, Oct. 2006.
[35] K. Yu and I. Oppermann, "Performance of UWB position estimation based on time-of-arrival measurements," in *Proc. Int. Workshop Ultra Wideband Syst.*, Oulu, Finland, May 2004, pp. 400–404.
[36] N. Maaref, P. Millot, C. Pichot, and O. Picon, "Through-the-wall radar using multiple UWB antennas," in *Proc. IET Int. Conf. Radar Syst.*, Oct. 2007, pp. 1–4.
[37] B. Alavi and K. Pahlavan, "Modeling of the TOA-based distance measurement error using UWB indoor radio measurements," *IEEE Commun. Lett.*, vol. 10, no. 4, pp. 275–277, Apr. 2006.
[38] A. Conti, M. Guerra, D. Dardari, N. Decarli, and M. Z. Win, "Network experimentation for cooperative localization," *IEEE J. Sel. Areas Commun.*, vol. 30, no. 2, pp. 467–475, Feb. 2012.
[39] S. Maranò, W. M. Gifford, H. Wymeersch, and M. Z. Win, "NLOS identification and mitigation for localization based on UWB experimental data," *IEEE J. Sel. Areas Commun.*, vol. 28, no. 7, pp. 1026–1035, Sep. 2010.
[40] J. Salmi and A. F. Molisch, "Propagation parameter estimation, modeling and measurements for ultrawideband MIMO radar," *IEEE Trans. Antennas Propag.*, vol. 59, no. 11, pp. 4257–4267, Nov. 2011.
[41] L. Ulander and T. Martin, "Bistatic ultra-wideband SAR for imaging of ground targets under foliage," in *Proc. IEEE Int. RadarCon*, Arlington, VA, USA, May 2005, pp. 419–423.
[42] S. Nag and M. Barnes, "A moving target detection filter for an ultra-wideband radar," in *Proc. IEEE Int. RadarCon*, Huntsville, AL, USA, May 2003, pp. 147–153.
[43] P. K. Dutta, A. K. Arora, and S. B. Bibyk, "Towards radar-enabled sensor networks," in *Proc. IEEE Inf. Process. Sensor Netw.*, Nashville, TN, USA, Apr. 2006, pp. 467–474.
[44] M. Sato and K. Yoshida, "Bistatic UWB radar system," in *Proc. IEEE Int. Conf. Ultra-Wideband*, Singapore, Sep. 2007, pp. 62–65.
[45] S. Bartoletti, M. Guerra, and A. Conti, "UWB passive navigation in indoor environment," in *Proc. 4th Int. Symp. Appl. Sci. Biomed. Commun. Technol.*, Barcelona, Spain, Oct. 2011, pp. 1–5.
[46] D. Dardari, R. D'Errico, C. Roblin, A. Sibille, and M. Z. Win, "Ultrawide bandwidth RFID: The next generation?" *Proc. IEEE*, vol. 99, no. 7, pp. 1570–1582, Jul. 2010.
[47] S. Bartoletti, A. Conti, A. Giorgetti, and M. Z. Win, "Sensor radar networks for indoor tracking," *IEEE Wireless Commun. Lett.*, vol. 3, no. 2, pp. 157–160, Apr. 2014.
[48] S. Bartoletti, W. Dai, A. Conti, and M. Z. Win, "A mathematical model for wideband ranging," *IEEE J. Sel. Topics Signal Process.*, vol. 9, no. 2, pp. 216–228, Mar. 2015.
[49] D. G. Brennan, "Linear diversity combining techniques," *Proc. IRE*, vol. 47, no. 6, pp. 1075–1102, Jun. 1959.
[50] J. H. Winters, "Optimum combining in digital mobile radio with cochannel interference," *IEEE J. Sel. Areas Commun.*, vol. SAC-2, no. 4, pp. 528–539, Jul. 1984.
[51] M. Z. Win, N. C. Beaulieu, L. A. Shepp, B. F. Logan, and J. H. Winters, "On the SNR penalty of MPSK with hybrid selection/maximal ratio combining over IID Rayleigh fading channels," *IEEE Trans. Commun.*, vol. 51, no. 6, pp. 1012–1023, Jun. 2003.
[52] A. Conti, W. M. Gifford, M. Z. Win, and M. Chiani, "Optimized simple bounds for diversity systems," *IEEE Trans. Commun.*, vol. 57, no. 9, pp. 2674–2685, Sep. 2009.
[53] A. F. Molisch and M. Z. Win, "MIMO systems with antenna selection—An overview," *IEEE Microw. Mag.*, vol. 5, no. 1, pp. 46–56, Mar. 2004.
[54] A. F. Molisch *et al.*, "A comprehensive standardized model for ultrawideband propagation channels," *IEEE Trans. Antennas Propag.*, vol. 54, no. 11, pp. 3151–3166, Nov. 2006.
[55] A. Safaai-Jazi, S. M. Riad, A. Muqaibel, and A. Bayram, "Report on through-the-wall propagation and material haracterization," carried out in the framework of the DARPA NETEX program "Ultra-wideband propagation measurements and channel modeling," Nov. 2002.
[56] J. Aspnes, D. Goldenberg, and Y. R. Yang, "On the computational complexity of sensor network localization," in *Proc. Int. Workshop Algorithmic Aspects Wireless Sensor Netw.*, Turku, Finland, Jul. 2004, pp. 32–44.
[57] D. E. Knuth, *The Art of Computer Programming, Volume 3: (2nd Ed.) Sorting and Searching*. Redwood City, CA, USA: Addison-Wesley, 1998.
[58] N. Balakrishnan and C. D. Lai, *Continuous Bivariate Distributions*, 2nd ed. Berlin, Germany: Springer-Verlag, 2009.
[59] M. Hollander and D. A. Wolfe, *Nonparametric Statistical Method*. Hoboken, NJ, USA: Wiley, 1973.
[60] E. Paolini, A. Giorgetti, M. Chiani, R. Minutolo, and M. Montanari, "Localization capability of cooperative anti-intruder radar systems," *EURASIP J. Adv. Signal Process.*, vol. 2008, no. 1, pp. 726 854-1–726 854-14, Apr. 2008.
[61] D. Dardari, C.-C. Chong, and M. Z. Win, "Threshold-based time-of-arrival estimators in UWB dense multipath channels," *IEEE Trans. Commun.*, vol. 56, no. 8, pp. 1366–1378, Aug. 2008.
[62] B. Boudamouz, P. Millot, and C. Pichot, "Through the wall MIMO radar detection with stepped frequency waveforms," in *Proc. EuRAD Conf.*, Paris, France, Sep. 2010, pp. 400–402.

Stefania Bartoletti (S'12) received the Laurea degree (*summa cum laude*) in electronics and telecommunications engineering from the University of Ferrara, Ferrara, Italy, in 2011, where she is currently working toward the Ph.D. degree.

Since 2010, she has been a Research Collaborator with the Wireless Communication and Localization Network Laboratory, University of Ferrara. From September 2013 to August 2014, she was a visiting Ph.D. student with the Laboratory for Information and Decision Systems, Massachusetts Institute of Technology, Cambridge, MA, USA. Her research interests include theory and experimentation of passive localization and tracking networks, particularly with application to wireless sensor radar and radio frequency identification systems.

Ms. Bartoletti served as a reviewer for numerous IEEE journals and international conferences.

Andrea Giorgetti (S'98–M'04–SM'13) received the Dr.Ing. degree (*summa cum laude*) in electronic engineering and the Ph.D. degree in electronic engineering and computer science from the University of Bologna, Bologna, Italy, in 1999 and 2003, respectively.

He is an Associate Professor with the University of Bologna. From 2003 to 2005, he was a Researcher with the National Research Council. During spring 2006, he was with the Laboratory for Information and Decision Systems (LIDS), Massachusetts Institute of Technology (MIT), Cambridge, MA, USA. Since then, he has been a Research Affiliate for LIDS, MIT. His research interests include ultrawide bandwidth communications systems, active and passive localization, wireless sensor networks, and cognitive radio.

Dr. Giorgetti was the Technical Program Cochair of the Cognitive Radio and Networks Symposium at the IEEE International Conference on Communications (ICC), Budapest, Hungary, June 2013, and the Cognitive Radio and Networks Symposium at the IEEE Global Communications Conference (Globecom), Atlanta, GA, USA, December 2013. He was a Technical Program Cochair of the Wireless Networking Symposium at the IEEE International Conference on Communications (ICC), Beijing, China, May 2008 and the MAC track at the IEEE Wireless Communications and Networking Conference (WCNC), Budapest, Hungary, April 2009. He is an Editor for the IEEE TRANSACTIONS ON WIRELESS COMMUNICATIONS and for the IEEE COMMUNICATIONS LETTERS.

Moe Z. Win (S'85–M'87–SM'97–F'04) received both the Ph.D. in Electrical Engineering and the M.S. in Applied Mathematics as a Presidential Fellow at the University of Southern California (USC) in 1998. He received the M.S. in Electrical Engineering from USC in 1989 and the B.S. (*magna cum laude*) in Electrical Engineering from Texas A&M University in 1987.

He is a Professor at the Massachusetts Institute of Technology (MIT) and the founding director of the Wireless Communication and Network Sciences Laboratory. Prior to joining MIT, he was with AT&T Research Laboratories for five years and with the Jet Propulsion Laboratory for seven years. His research encompasses fundamental theories, algorithm design, and experimentation for a broad range of real-world problems. His current research topics include network localization and navigation, network interference exploitation, intrinsic wireless secrecy, adaptive diversity techniques, and ultra-wide bandwidth systems.

Professor Win is an elected Fellow of the AAAS, the IEEE, and the IET, and was an IEEE Distinguished Lecturer. He was honored with two IEEE Technical Field Awards: the IEEE Kiyo Tomiyasu Award (2011) and the IEEE Eric E. Sumner Award (2006, jointly with R. A. Scholtz). Together with students and colleagues, his papers have received numerous awards, including the IEEE Communications Society's Stephen O. Rice Prize (2012), the IEEE Aerospace and Electronic Systems Society's M. Barry Carlton Award (2011), the IEEE Communications Society's Guglielmo Marconi Prize Paper Award (2008), and the IEEE Antennas and Propagation Society's Sergei A. Schelkunoff Transactions Prize Paper Award (2003). Highlights of his international scholarly initiatives are the Copernicus Fellowship (2011), the Royal Academy of Engineering Distinguished Visiting Fellowship (2009), and the Fulbright Fellowship (2004). Other recognitions include the International Prize for Communications Cristoforo Colombo (2013), the *Laurea Honoris Causa* from the University of Ferrara (2008), the Technical Recognition Award of the IEEE ComSoc Radio Communications Committee (2008), and the U.S. Presidential Early Career Award for Scientists and Engineers (2004).

Dr. Win was an elected Member-at-Large on the IEEE Communications Society Board of Governors (2011–2013). He was the Chair (2004–2006) and Secretary (2002–2004) for the Radio Communications Committee of the IEEE Communications Society. Over the last decade, he has organized and chaired numerous international conferences. He is currently an Editor-at-Large for the IEEE WIRELESS COMMUNICATIONS LETTERS. He served as Editor (2006–2012) for the IEEE TRANSACTIONS ON WIRELESS COMMUNICATIONS, and as Area Editor (2003–2006) and Editor (1998–2006) for the IEEE TRANSACTIONS ON COMMUNICATIONS. He was Guest-Editor for the PROCEEDINGS OF THE IEEE (2009) and for the IEEE JOURNAL ON SELECTED AREAS IN COMMUNICATIONS (2002).

Andrea Conti (S'99–M'01–SM'11) received the Laurea degree (*summa cum laude*) in telecommunications engineering and the Ph.D. degree in electronic engineering and computer science from the University of Bologna, Bologna, Italy, in 1997 and 2001, respectively.

He is an Associate Professor with the University of Ferrara, Ferrara, Italy. Prior to joining the University of Ferrara, he was with the Consorzio Nazionale Interuniversitario per le Telecomunicazioni and with the Istituto di Elettronica e di Ingegneria dell'Informazione e delle Telecomunicazioni, Consiglio Nazionale delle Ricerche. In the Summer of 2001, he was with the Wireless Systems Research Department at AT&T Research Laboratories. Since 2003, he has been a frequent visitor to the Wireless Communication and Network Sciences Laboratory, Massachusetts Institute of Technology, Cambridge, MA, USA, where he presently holds the Research Affiliate appointment. He is a coauthor of *Wireless Sensor and Actuator Networks: Enabling Technologies, Information Processing and Protocol Design* (Elsevier, 2008). His research interests involve theory and experimentation of wireless systems and networks, including network localization, adaptive diversity communications, cooperative relaying techniques, and network secrecy. He received the HTE Puskás Tivadar Medal and coreceived the IEEE Communications Society's Stephen O. Rice Prize and the IEEE Communications Society's Fred W. Ellersick Prize.

Dr. Conti is serving as an Editor for the IEEE WIRELESS COMMUNICATIONS LETTERS and served as an Associate Editor for the IEEE TRANSACTIONS ON WIRELESS COMMUNICATIONS, as an Editor for the IEEE COMMUNICATIONS LETTERS, and as a Guest Editor for the EURASIP *Journal on Advances in Signal Processing* (Special Issue on Wireless Cooperative Networks, 2008). He has organized and chaired a number of IEEE conferences. He was elected Chair of the IEEE Communications Society's Radio Communications Technical Committee. He is an elected Fellow of the Institute of Engineering and Technology and has been selected as an IEEE Distinguished Lecturer.